Molecular Order in High-Efficiency Polymer/Fullerene Bulk Heterojunction Solar Cells

Matthew R. Hammond,[†] R. Joseph Kline,[†] Andrew A. Herzing,[†] Lee J. Richter,[†] David S. Germack,[†] Hyun-Wook Ro,[†] Christopher L. Soles,[†] Daniel A. Fischer,[†] Tao Xu,[‡] Luping Yu,[‡,*] Michael F. Toney,[§] and Dean M. DeLongchamp[†,*]

[†]National Institute of Standards and Technology, Gaithersburg, Maryland 20899, United States, [‡]Department of Chemistry and the James Frank Institute, University of Chicago, Chicago, Illinois 60637, United States, and [§]Stanford Synchrotron Radiation Lightsource, Menlo Park, California 94025, United States

ABSTRACT We report quantitative measurements of ordering, molecular orientation, and nanoscale morphology in the active layer of bulk heterojunction (BHJ) organic photovoltaic cells based on a thieno[3,4-*b*]thiophene-*alt*-benzodithiophene copolymer (PTB7), which has been shown to yield very high power conversion efficiency when blended with [6,6]-phenyl-C71-butyric acid methyl ester ($PC_{71}BM$). A surprisingly low degree of order was found in the polymer—far lower in the bulk heterojunction than in pure PTB7. X-ray diffraction data yielded a nearly full orientation distribution for the polymer π-stacking direction within well-ordered regions, revealing a moderate preference for π-stacking in the vertical direction ("face-on"). By combining molecular orientation information from polarizing absorption spectroscopies with the orientation distribution of ordered material from diffraction, we propose a model describing the PTB7 molecular orientation distribution (ordered and disordered), with the fraction of ordered polymer as a model parameter. This model shows that only a small fraction ($\approx$20%) of the polymer in the PTB7/$PC_{71}BM$ blend is ordered. Energy-filtered transmission electron microscopy shows that the morphology of PTB7/$PC_{71}BM$ is composed of nanoscale fullerene-rich aggregates separated by polymer-rich regions. The addition of diiodooctane (DIO) to the casting solvent, as a processing additive, results in smaller domains and a more finely interpenetrating BHJ morphology, relative to blend films cast without DIO.

KEYWORDS: organic photovoltaics · bulk heterojunction · crystallinity · orientation · polymers

Polymer-based solar cells (PSCs) have been the focus of intense development due to their potential for producing low-cost electricity using earth-abundant materials.[1] Much effort has focused on bulk heterojunction (BHJ) devices,[2] in which finely interdispersed percolating networks of a photon-absorbing electron donor polymer and an electron-accepting species (most often a soluble fullerene derivative) are created dynamically upon casting a solution of the blend components. A burst of creative synthetic chemistry in the past decade has seen the development of new absorber polymers[3−7] with purposefully engineered HOMO and LUMO levels in order to optimize band gap overlap with the solar spectrum and to increase the device open circuit voltage (V_{oc}),[8] leading to a steady upward trend in reported solar cell efficiencies. Many such polymers employ an alternating copolymer architecture; a particularly promising family are composed of alternating ester-substituted thieno[3,4-*b*]-thiophene and benzodithiophene units (PTB).[7,9,10] BHJ devices based on PTB7 (see Figure 1) and [6,6]-phenyl-C71-butyric acid methyl ester ($PC_{71}BM$), for instance, have shown power conversion efficiencies (PCE) in excess of 7%.[10] In this report, we determine the overall degree of molecular order (crystallinity) and degree of molecular orientation of the PTB7 in such blend films and find the polymer to be more disordered than what one might initially expect from such a high-performance system.

It is generally accepted that BHJ device performance is a strong function of a diversity of morphological details at multiple length scales.[11] One aspect of an optimal BHJ morphology requires that the absorber polymer molecules be arranged in such a way as to provide high charge mobility, allowing holes to quickly reach the anode and minimizing losses due to recombination. Conventional wisdom has posited that achieving increased crystallinity of the polymer absorber is of paramount importance.[12−16] For BHJ PSCs based on poly(3-hexylthiophene) (P3HT), for example, appropriate thermal or solvent annealing treatments that improve the crystallinity of P3HT indeed yield greatly improved device performance.[14−16] Given the morphological heterogeneity inherent in polymer semiconductors, forming a precise picture of how microstructure influences charge transport remains a challenging task.[17]

* Address correspondence to dean.delongchamp@nist.gov, lupingyu@uchicago.edu.

Received for review August 3, 2011 and accepted September 22, 2011.

Published online September 22, 2011
10.1021/nn202951e

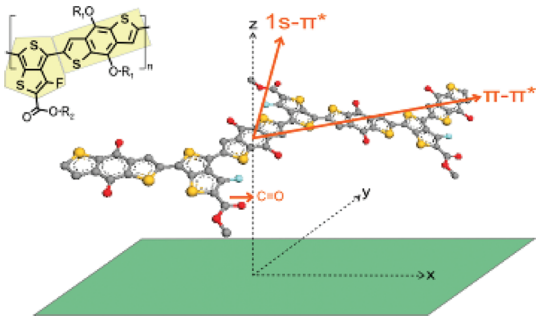

Figure 1. (Inset) Molecular structure for PTB7; alkyl side chains: $R_1 = R_2$ = 2-ethylhexyl. In the molecular model shown, in which the alkyl side chains are omitted, the orientation (with respect to the molecule) of the transition dipoles relevant to the spectroscopy experiments are diagrammed in orange.

Any such understanding must consider a host of factors such as the distribution of the polymer between ordered and disordered regions, and the molecular orientation distributions within those regions. Recent work using advanced X-ray diffraction line shape analysis to characterize the degree of structural order within the crystalline regions of poly[2,5-bis(3-alkylthiophen-2-yl)thieno(3,2-*b*)thiophene] (PBTTT) has shown that even in PBTTT, known to produce outstandingly high degrees of order relative to other semiconducting polymers,[18−20] large fluctuations in molecular spacing in the $\pi-\pi$ stacking direction cause the ordered regions to be highly paracrystalline.[21] Additionally, measurement of the absolute content of crystalline[22] (or paracrystalline) *versus* disordered material has remained elusive despite intensive efforts. Recent steps toward this goal have allowed the comparison of the relative fraction of ordered material between several polymer semiconductor films subjected to varying thermal treatments by integrating the total scattered intensity (over all orientations) for a given (*hkl*) reflection in grazing-incidence X-ray diffraction (GIXD) measurements.[23−25]

An early report demonstrated a qualitative preference for the crystalline regions of PTB in PTB:PCBM solar cells to be preferentially oriented with their $\pi-\pi$ stacking direction nominally in the vertical (out-of-plane) direction.[26] This so-called "face-on" (or "plane-on") orientation may contribute to enhanced vertical charge transport and, therefore, may be a signature of materials yielding high-performance devices. (In contrast, P3HT:PCBM devices show a predominance of "edge-on" molecular orientation.)[23,27] However, thorough analysis of GIXD experiments using an area detector can furnish quantitative information on texture (*i.e.*, a nearly full orientation distribution function for a given reflection) for regions ordered enough to give rise to scattering.[28] Polarizing spectroscopy techniques such as variable angle spectroscopic ellipsometry (SE), near-edge X-ray absorption fine structure (NEXAFS), and polarized infrared (p-IR) absorption can probe various aspects of molecular orientation, as well,[29] but with no specificity for crystalline *versus* disordered film regions. In this paper, using GIXD and the polarizing spectroscopies just mentioned, we thoroughly characterize orientation and order in PTB7:$PC_{71}BM$ blend films, as well as for neat PTB7 films. These techniques provide complementary information, and careful analysis of the data in aggregate allows us to construct a model of the full PTB7 orientation distribution which predicts that the fraction of ordered polymer within the BHJ active layer is only approximately 21%. An important implication for synthetic design, therefore, is that a polymer absorber does not necessarily have to be highly crystalline to achieve high performance in OPV cells. Indeed, there is at least one other example of a polymer absorber that functions in BHJ devices with impressive PCE[30] despite being characterized by little crystalline ordering.[31−33]

Additionally, we explore the nanoscale blend film morphology, including the effect of the processing additive diiodooctane (DIO) on that morphology. PTB7:$PC_{71}BM$ BHJ devices cast from *o*-dichlorobenzene (DCB) improved from 6.2 to 7.2% PCE upon addition of a volume fraction of 3% of DIO.[10] Whereas the GIXD and polarizing spectroscopy experiments showed little difference between blends cast with or without DIO, energy-filtered transmission electron microscopy (EF-TEM) results show that DIO addition causes the BHJ morphology to be more finely interpenetrating, relative to blend films spun without DIO. The action of DIO in the PTB7:$PC_{71}BM$ system is thus quite different from its effect in some other polymer:fullerene systems, where the DIO causes an otherwise phase-mixed system to separate into nanoscale polymer-rich and fullerene-rich regions.[34,35]

RESULTS AND DISCUSSION

PTB7 was synthesized as reported previously,[10,36] and neat PTB7 and PTB7:$PC_{71}BM$ blend films were spincast from *o*-dichlorobenzene (DCB) solutions. The films were then subjected to a battery of morphology characterization techniques: GIXD, SE, p-IR, NEXAFS, and EF-TEM. For blend films, data were collected from films prepared with and without the addition of a volume fraction of 3% of DIO in the DCB casting solvent.

GIXD. The molecular packing structure, size, and orientation of crystalline domains within the neat and blend films were probed with GIXD, results from which are presented in Figure 2. In both the neat PTB7 film (Figure 2a) and the blends (*e.g.*, Figure 2b, for the blend processed with DIO), a number of broad arcs of scattering arise. Primarily in the in-plane (q_{xy}) direction, a reflection is observed from the (100) crystal direction at $q \approx 0.36$ Å^{-1} (lamellar stacking of the backbones in the alkyl side chain direction with a periodicity of *ca.* 17 Å), and primarily in the out-of-plane direction, a broad arc is observed at $q \approx 1.61$ Å^{-1} due to the (010)

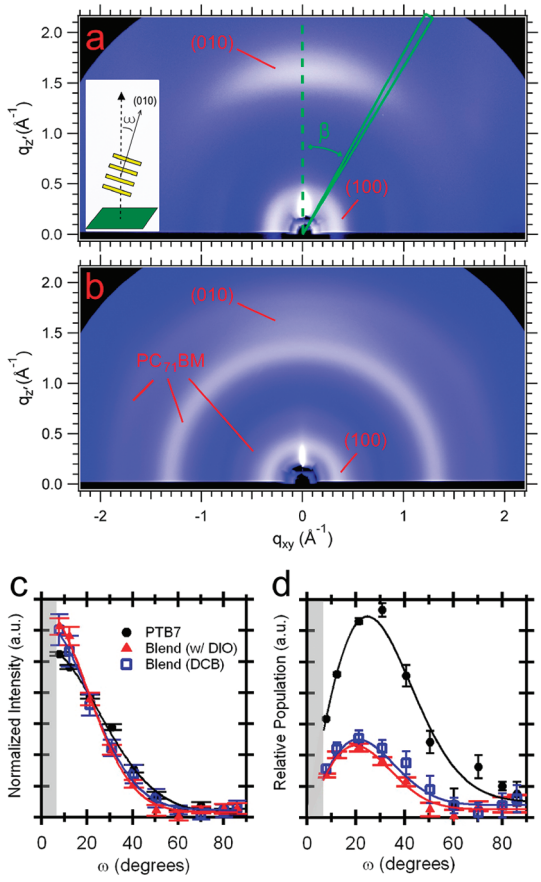

Figure 2. GIXD detector images for (a) neat PTB7 and (b) PTB7:$PC_{71}BM$ blend (with DIO) films. Note that the intensity (color) scales for the two images are not the same, and the vertical axes are labeled $q_{z'}$ to reflect the fact that the scattering vector measured along the detector meridian ($q_{xy} \approx 0$) is not exactly parallel to the sample *z*-direction. The detector angle β is not equivalent to the polar angle ω (diagrammed in the inset). (c) Pole figures for the (010) reflection for neat PTB7 (black circles) and for PTB7:$PC_{71}BM$ blend films prepared with (red triangles) and without (blue squares) DIO processing additive. The error bars are calculated from the estimated standard deviations from the peak fitting coefficients. The data are normalized by the total scattered intensity for each given sample. (d) Geometrically corrected orientation distribution functions (symbols the same as in (c)). The data are scaled by the film thickness, beam path length, and polymer volume fraction, showing that the neat film has significantly higher crystalline content relative to the blend films.

(π-stacking) reflection. These results are in qualitative agreement with those obtained from GIXD experiments on related PTB-based polymers.[26,37] For the blend films, isotropic rings due to $PC_{71}BM$ occur at $q \approx 0.65$, 1.33, and 1.86 $Å^{-1}$ (see Supporting Information). The GIXD pattern from the blend film processed without DIO is qualitatively very similar to Figure 2b (also see Supporting Information), showing that there are almost no changes in the local PTB7 structure on processing with DIO.

In order to extract quantitative information about the distribution of crystallite orientations, pole figures[38] were constructed from the detector images. In particular, we focus on the distribution of (010) orientations as a function of ω, the polar angle between a particular PTB7 crystallite's (010) direction and the sample normal. Figure 2c shows the integrated peak area (over *q*) arising from diffraction associated with crystallites with a given orientation, ω. Construction of pole figures from such detector images requires several corrections,[28] and in order to separate contributions from multiple overlapping scattering peaks (especially for the blend films), wedge cuts were taken at several detector angles, β (diagrammed in Figure 2a), and the area of the (010) peak was obtained by multiple-peak fitting. This process is described in detail in the Supporting Information, but it is worth noting a few details here. Due to the geometry of the GIXD experiment and the fact that the surface of the Ewald sphere is curved, the detector angle (β) is not exactly equivalent to the polar angle (ω). The necessary correction becomes more important as β approaches 0. For example, at $q = 1.61$ $Å^{-1}$ (the (010) peak position), $\beta = 0$ corresponds to $\omega \approx 7.2°$, so we are unable to measure the intensity for orientations $\omega < 7.2$. The inaccessible ω range is shown by the gray-shaded areas in Figure 2c,d. Collecting data for $\omega < 7.2$ would require a second scattering experiment involving the measurement of a rocking curve near the specular ($q_{xy} = 0$) condition. Unfortunately, at the large values of *q* (*i.e.*, relatively large angles) necessary to probe the (010) peak, scattering signal rarely rises above background in such an experiment. It is therefore possible that we are missing some population of crystals that are highly (010) oriented along the substrate normal. However, such a population appears highly unlikely, given the relative lack of strong polymer chain orientation that was found from the polarizing spectroscopy experiments, as will be discussed below. We therefore proceed assuming that the pole figures can be smoothly extrapolated to $\omega = 0$.

Also worthy of mention are the observed (010) peak line widths. For the neat PTB7 film, the (010) peak width is at a minimum for small β angles, and the width increases as β increases. Inputting these peak widths into the Scherrer formula[39] yields average coherence lengths ($L_{c,010}$) for the crystalline domains of the various orientations. The coherence length of the most vertically oriented crystals is only *ca.* 1.7 nm, or approximately 4.5 $\pi-\pi$ stacked chains, and drops to *ca.* 1.2 nm ($\approx$3 $\pi-\pi$ stacks) for crystals oriented with $\omega \geq 30°$. $L_{c,010}$ values for the blend films are similarly very short: 1 to 1.5 nm. As a reference point for comparison, $L_{c,010}$ for P3HT crystals in a P3HT:PCBM blend was found recently to be approximately 5 nm ($\approx$16 $\pi-\pi$ stacks).[40] Note also that the (100) Scherrer correlation length for the PTB7 blends is *ca.* 5 nm ($\approx$3 *d*-spacings), whereas typical values for the P3HT (100) in the P3HT:PCBM system are *ca.* 16 nm ($\approx$9 *d*-spacings).[40] We note that analysis of a single (*hkl*) reflection peak using the Scherrer equation allows only the calculation of a scattering coherence length (distance over which unit

cells are spatially correlated), which includes contributions not only from finite crystallite size but also from non-uniform crystal strain and paracrystallinity. On the basis of similar polymers, the cause is most likely paracrystallinity,[21] but whatever the cause, the PTB7 correlation lengths in the neat and blend films are notable for being very short.[33]

The pole figures presented in Figure 2c were normalized by the total (010) scattered intensity for each film (integrated over all observable ω) in order to facilitate comparison between samples. The functional forms of the pole figures for the neat PTB7 and blend films are nearly identical, showing a strong preference for π-stacking in directions which make a relatively small angle with the film normal. The solid lines in Figure 2c are fits to Gaussian line shapes centered at $\omega = 0$ (although there is no obvious physical reason for the distribution to follow this functional form). To correct for geometrical effects, the peak area data must be multiplied by a factor of (sin ω). More discussion of this point is provided in the Supporting Information and elsewhere.[25]

For the orientation distributions shown in Figure 2d, the geometrical correction (sin ω) was applied, and the (010) peak areas were normalized by the X-ray exposure, the film thickness, beam footprint size, and polymer volume fraction. These corrections permit the comparison of absolute volume of scattering domains within the respective (neat polymer *versus* blend) films.[23] Integration of these relative distribution functions over ω yields the interesting result that the polymer within the blend with DIO has 3.1 (±0.5) times less overall crystalline content than the PTB7 neat film,[41] and the corresponding figure for the non-DIO blend film is a factor of 2.5 (±0.5). Within the experimental uncertainties, there is no difference in crystallinity resulting from the DIO additive. The second moments, $\langle\cos^2\omega\rangle$, of the distributions in Figure 2d are reported in Table 1. To give a somewhat more intuitive figure, Table 1 also lists equivalent average angles, $\langle\omega\rangle_\delta$, where the delta subscript denotes that a delta function orientation distribution at that angle would give the same $\langle\cos^2\omega\rangle$ value. The orientation distributions are quite broad (fwhm ≈ 35°) and show that the average crystal in the neat and blend films is oriented at angles near ≈33° from the film vertical, a fact that is not obvious from simple inspection of the scattering patterns.

Polarizing Spectroscopies. For samples with no preferred in-plane orientation, polarizing spectroscopy techniques can be used to determine the orientation average, $\langle\cos^2\theta_\mu\rangle$, of the relevant transition dipole vector, μ, where θ_μ is the angle between μ and the sample normal. The value of $\langle\cos^2\theta_\mu\rangle$ does not contain information about the functional form of the orientation distribution; for instance, a sample in which μ is isotropically oriented and a sample in which μ is perfectly oriented at the magic angle ($\theta_\mu \approx 54.7°$) will both exhibit $\langle\cos^2\theta_\mu\rangle = 1/3$. As was observed in the GIXD results, only slight differences were observed in the spectroscopy experiments when comparing blends prepared with and without DIO.

TABLE 1. Figures of Merit for Measures of Polymer Orientation

	GIXD		SE			p-IR (νC=O)	
	$\langle\cos^2\omega\rangle$	$\langle\omega\rangle_\delta$[a]	$\varepsilon''_{zz}/\varepsilon''_{x\text{-}y}$	$\langle\cos^2\theta_{bb}\rangle$	$\langle\theta_{bb}\rangle_\delta$[a]	A_p/A_s	$\langle\theta_{C=O}\rangle_\delta$[a]
PTB7	0.68	35	0.22	0.10	72	0.34	60
blend	0.72	32	0.42	0.17	65	0.31	59
blend (w/o DIO)	0.69	34	0.42	0.17	65	0.32	58

	NEXAFS: C 1s-π^*			model		
	R	$\langle\cos^2\theta_\pi\rangle$	$\langle\theta_\pi\rangle_\delta$[a]	$\langle\cos^2\theta_\pi\rangle$	$\langle\theta_\pi\rangle_\delta$[a]	$\langle\theta_{C=O}\rangle_\delta$[a]
PTB7[b]	−0.16	0.42	50	0.48	46	66
blend[b]	0.14	0.26	59	0.34	54	64
blend, w/o DIO[b]	0.08	0.29	57	0.34	54	64
PTB7 (bottom)[b]	−0.39	0.55	42			

[a] Average tilt angle (degrees) assuming a delta function equivalent orientation function. [b] NEXAFS orientation data are from the film top surface except where specified.

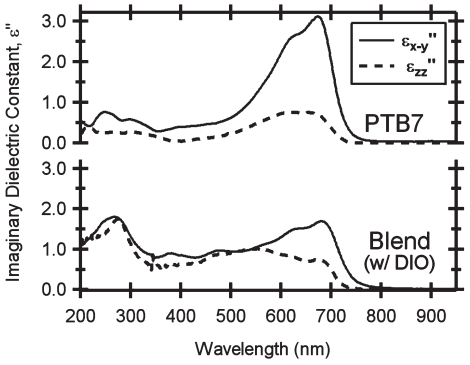

Figure 3. Uniaxial dielectric functions from fits of SE data. In-plane ($\varepsilon''_{x\text{-}y}$, solid lines) and out-of-plane (ε''_{zz}, dashed lines) components of the model imaginary dielectric functions are shown for the neat PTB7 and blend (with DIO) films.

Spectroscopic ellipsometry experiments were performed to determine the average orientation of the polymer backbones. In an SE experiment, the complex reflectance ratio (amplitude ratio and phase shift) for light polarized parallel or perpendicular to the plane of incidence is measured as a function of incident angle and wavelength (over the UV/visible/near-IR range). Model dielectric functions for the films were then calculated by iterative fitting of SE data. Acceptable fits could only be obtained by employing uniaxial models, that is, with different dielectric functions for the in-plane and out-of-plane directions. The imaginary (absorptive) parts of the calculated dielectric functions, $\varepsilon''_{x\text{-}y}$ (in-plane) and ε''_{zz} (out-of-plane), are shown

in Figure 3 for the neat PTB7 and blend films. (We use the notation $\varepsilon''_{x\text{-}y}$ to reflect the fact that, for spin-coated films such as these, there is no preferred in-plane orientation, *i.e.*, $\varepsilon''_{xx} = \varepsilon''_{yy}$.) ZINDO calculations showed that the transition dipole moment for the $\pi-\pi^*$ excitation at *ca.* 682 nm lies along the nominal polymer chain backbone axis (see the Supporting Information). Therefore, the dichroic ratio ($R_{SE} \equiv \varepsilon''_{zz}/\varepsilon''_{x\text{-}y}$) for that transition is a quantitative measure of the average polymer backbone orientation. From this ratio, the second moment of the backbone orientation distribution, $\langle \cos^2 \theta_{bb} \rangle$, can be calculated, where θ_{bb} is the angle that a given backbone makes with the film normal. As reported in Table 1, the observed SE dichroic ratios of 0.22 and 0.42 for neat film and blends, respectively, indicate that there is preferential backbone alignment in the film plane. Such behavior is typical of semiconducting polymers.[29,42,43] As points of comparison, an as-cast regioregular P3HT film was found to have $\varepsilon''_{zz}/\varepsilon''_{x\text{-}y} = 0.11$, that is, significantly more highly in-plane orientation than those observed here, whereas an as-cast regiorandom P3HT (known to be amorphous) film had $\varepsilon''_{zz}/\varepsilon''_{x\text{-}y} = 0.60$.[29]

Infrared spectroscopy has a long history of providing important structural information, and for thin film samples mounted at Brewster's angle with respect to the beam and measured in transmission, the ratio of absorbance for p-polarized and s-polarized light gives a quantitative measure of orientation of the relevant vibrational transition.[29] Figure 4 shows vibrational spectra in the region of the ester C═O stretching bands observed in the neat PTB7 and blend films. Two distinct C═O stretches are evident in pure PTB7, at 1704 and 1724 cm^{-1}, due to the ester group located on the polymer thienothiophene subunit. The structure drawn in the inset of Figure 1 shows the C═O bond in a *cis* configuration with respect to the adjacent C═S bond. A calculation using Gaussian[44] suggests that this conformational isomer is isoenergetic with that in which the C═O and C═S bonds are *trans* to each other, but that the C═O stretching energies are significantly split from one another. For the blend film, the ester νC═O absorption from $PC_{71}BM$ overlaps strongly with the PTB7 νC═O at 1726 cm^{-1}. Thus, for comparing C═O bond angles in PTB7 *versus* blend, we calculate the dichroic ratio, A_p/A_s, only for the 1704 cm^{-1} peak (listed in Table 1). Direct interpretation of this dichroic ratio is difficult since the IR data do not allow a unique determination of the relevant dielectric tensor.

Instead, a calibration curve (A_p/A_s *versus* transition dipole tilt angle) must be forward-simulated for each possible value of $\langle \cos^2 \theta_\mu \rangle$, taking into account the proper film refractive index. Details of this procedure and calibration curves are provided in the Supporting Information. As reported in Table 1, the polymer C═O bonds in the neat and blend films show only slight preference for in-plane orientation (≈58−60° from vertical *versus* the magic angle, 54.7°, for an isotropic distribution). For comparison, if the polymer was oriented with a uniquely face-on orientation, the C═O bonds would all lie in-plane, that is, with $\theta_{C=O} = 90°$. Thus, there is very little preferential orientation of the ester C═O bonds.

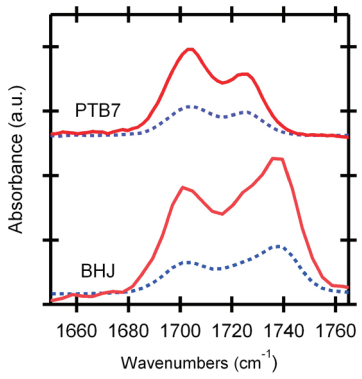

Figure 4. IR spectra of PTB7 and BHJ (with DIO) films in the C═O stretch region. Spectra from the different samples have been offset for clarity. Data using an s-polarized probe beam are shown as solid red lines; p-polarization spectra are dashed and blue.

The methylene antisymmetric stretch frequency is known to be sensitive to conformation,[45] and for both the neat PTB7 and blend films, the $\nu_a CH_2$ band lies at 2928 cm^{-1}, indicating a disordered, liquid-like environment among the alkyl side chains (data not shown). This is consistent with the short, branched nature of the 2-ethylhexyl units.

NEXAFS spectroscopy was performed to probe the orientation-induced dichroism of the PTB7 carbon 1s-π^* transition dipole, which lies perpendicular to the polymer-conjugated ring plane. Measurements were made in partial electron yield mode, imparting sensitivity to only the topmost few nanometers of the films analyzed. Analysis of films delaminated from their (silicon oxide) substrates was also performed in order to probe orientation at the substrate surface. However, polymer orientation data from the film bottom surface could only be obtained from PTB7 neat films, as the blend films exhibited a large enrichment of the fullerene component at the oxide interface, an effect which has also been observed previously in P3HT:PCBM blends.[46] The data on surface composition, as well as representative spectra as a function of photon angle of incidence, are shown in the Supporting Information. The dichroic ratio, R, is determined by extrapolating (to 0 and 90°) the linear relation between the sine squared of the incidence angle and the area of the polymer 1s-π^* peak.[47] The value of $\langle \cos^2 \theta_\pi \rangle$ is then calculated from R. Again note that the C 1s-π^* transition orientation angle, θ_π, is defined with respect to the film normal, and that an isotropic distribution would give $\langle \cos^2 \theta \rangle = 1/3$ or $\langle \theta \rangle_\delta \approx 54.7$ (=the magic angle). The measured R and $\langle \cos^2 \theta_\pi \rangle$ values, along with the

associated δ function distribution equivalent angles, are also listed in Table 1. The PTB7 neat film shows a slight preference for face-on orientation (average θ_π less than 54.7°) at both the top and bottom surfaces, whereas the blend films' top surfaces show a very slight "edge-on" preference (>54.7°). In general, however, it must be stressed that the most striking feature of these data is the absence of evidence for strong polymer orientation.

Morphology Model. Given that the various morphology probes described above yield information about nominally orthogonal aspects of the polymer orientation, we have constructed a simplified model to interpret the data in aggregate. The model assumes that the polymer in a given film (neat or blend) exists in either crystalline regions or in amorphous regions, the fractions of which are denoted p and $1 - p$, respectively. The amorphous regions, though not well ordered, are nonetheless almost certainly not perfectly isotropic. For example, although spin-coated films of regiorandom P3HT show no crystallinity, SE experiments showed $R_{SE,amorph}$ (*i.e.*, $\varepsilon''_{zz}/\varepsilon''_{x\text{-}y}$) to have a value of 0.6.[29] For the present morphology model, we initially assume this value holds for the amorphous regions of PTB7 and discuss below and in the Supporting Information the importance of this assumption. The model assumes that the polymer backbones within the crystalline regions are oriented exclusively in plane (*i.e.*, $R_{SE,xtal} = 0.0$). The (010) orientation distribution for the crystalline fraction is as obtained empirically from GIXD.

Using these assumptions, a combination of contributions from crystalline and amorphous polymer regions allows the calculation of p from the observed SE $R_{SE,total}$ ($=\varepsilon''_{zz}/\varepsilon''_{x\text{-}y}$) values. Using a linear effective medium approximation, the amorphous and crystalline regions of the film contribute to the overall dielectric function. Thus

$$R_{SE,total} = \frac{\varepsilon''_{zz,total}}{\varepsilon''_{xx,total}} = \frac{p \times \varepsilon''_{zz,xtal} + (1-p)\varepsilon''_{zz,amorph}}{p \times \varepsilon''_{xx,xtal} + (1-p)\varepsilon''_{xx,amorph}} \quad (1)$$

(Note that only the imaginary part of the dielectric function, $\varepsilon = \varepsilon' + i\varepsilon''$, is used in the calculation of R_{SE}.) While more sophisticated effective medium models have been developed,[48] they represent less than a 10% correction to the simple model for similar systems.[47] We further assume that, for each component (crystal or amorphous), the sum $\varepsilon''_{zz} + \varepsilon''_{xx} + \varepsilon''_{yy}$ is a constant (ε''_{xtal} or ε''_{amorph}). Simple algebraic manipulation then yields

$$p = \frac{\varepsilon''_{zz,amorph} - R_{SE,total} \times \varepsilon''_{xx,amorph}}{R_{SE,total}(\varepsilon''_{xx,xtal} - \varepsilon''_{xx,amorph}) - (\varepsilon''_{zz,xtal} - \varepsilon''_{zz,amorph})} \quad (2)$$

with

$$\varepsilon''_{xx,amorph} = \frac{\varepsilon''_{amorph}}{R_{SE,amorph} + 2}$$
$$\varepsilon''_{xx,xtal} = \frac{\varepsilon''_{xtal}}{R_{SE,xtal} + 2} \quad (3)$$

$$\varepsilon''_{zz,amorph} = \varepsilon''_{amorph} - 2 \times \varepsilon''_{xx,amorph}$$
$$\varepsilon''_{zz,xtal} = \varepsilon''_{xtal} - 2 \times \varepsilon''_{xx,xtal} \quad (4)$$

The absolute numbers input for the extinction coefficients ε''_{xtal} and ε''_{amorph} are arbitrary; only their ratio matters once the numbers are input into eqs 2−4. We set $\varepsilon''_{xtal}/\varepsilon''_{amorph} = 1.2$, the reasons for which are discussed in the Supporting Information. The predicted crystallinity values reported below are rather insensitive to the choice of this parameter, within a reasonable range (*e.g.*, $1.0 < \varepsilon''_{xtal}/\varepsilon''_{amorph} < 1.4$).[49]

The model predicts $p_{neat} = 0.54 \pm 0.05$ for the neat PTB7, and $p_{blend} = 0.21 \pm 0.02$ for the two blend films. These values give $p_{neat}/p_{blend} = 2.6 \pm 0.4$, which compares well with the estimates from the GIXD relative crystallinity analysis. In order to further evaluate the validity of this model, we calculate the orientation distribution functions for the π^* and C═O directors (see Supporting Information for calculation details) and compare the resulting average values for $\langle \cos^2 \theta_\pi \rangle$, $\langle \theta_\pi \rangle_\delta$, and $\langle \theta_{C=O} \rangle_\delta$ to the values observed experimentally (see Table 1). The model agrees quite well with the NEXAFS data for π^* director orientation at the film top surfaces, with the model and experimental $\langle \theta_\pi \rangle_\delta$ values being within only a handful of degrees of each other and with the model values capturing the observed trend of increasing $\langle \theta_\pi \rangle_\delta$ upon going from neat film to blend film. The neat PTB7 bottom surface shows more preferential out-of-plane orientation, suggesting that the oxide surface induces some enrichment of nominally face-on polymer content, some enrichment of crystalline content, or some combination of both. The model predictions for the C═O bond orientations also compare well against the experimental data, with reasonable agreement in both the average tilt angle $\langle \theta_{C=O} \rangle_\delta$ and the trend upon going from neat film to blend.

Thus, although the model rests upon somewhat restrictive assumptions, it is likely to capture many of the essential properties of the polymer orientation distribution, giving us confidence that the estimate, $p_{blend} = 0.21$, is in the correct neighborhood. In any case, the relative crystallinity estimate from GIXD ($p_{neat}/p_{blend} = 3.1 \pm 0.5$) puts an upper limit on p_{blend} of *ca.* 0.32 (in the extremely unlikely case that $p_{neat} = 1.0$). Allowing the input value of $R_{SE,amorph} = 0.6$ to vary by ±10% results in a range for p ($0.14 < p_{blend} < 0.26$). Alternatively, allowing $R_{SE,xtal}$ to rise to 0.1 from 0 increases p_{blend} to 0.26. Exploring combinations of reasonable values for these two parameters which yield p values

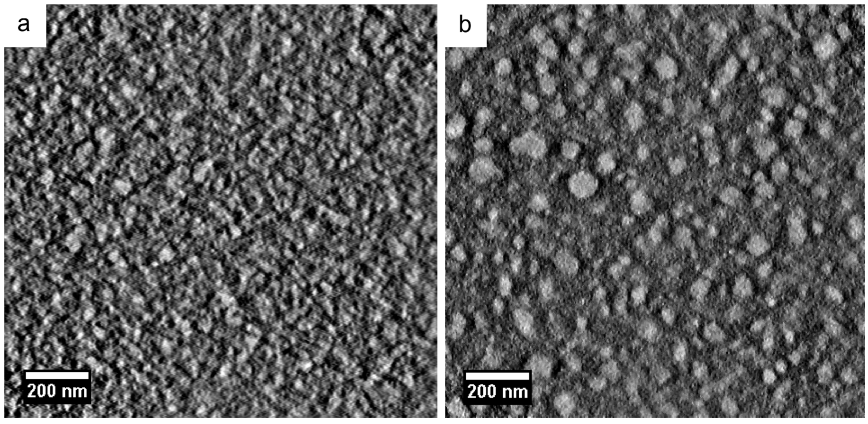

Figure 5. Results from EF-TEM tomography reconstructions showing *x-y* slices near the middle (in *z*, slice thickness ≈2 nm) of the blend film cast from DCB/DIO (a) and the blend cast from DCB only (b). $PC_{71}BM$-rich regions appear bright in these images, which highlight the fact that addition of DIO to the casting solvent results in a reduction in the average size of $PC_{71}BM$-rich domains.

that still satisfy ($p_{neat}/p_{blend} = 3.1 \pm 0.5$) confines p_{blend} to the range ($0.13 < p_{blend} < 0.28$). More discussion of this point can be found in the Supporting Information.

Nanoscale Morphology. The nanoscale morphology of the PTB7/$PC_{71}BM$ bulk heterojunction relates to its power conversion efficiency because it provides the three-dimensional framework through which excitons diffuse and charges are transported to electrodes. Previous TEM results for this system have been based on bright-field (BF) imaging, which revealed a dramatic effect between PTB7:$PC_{71}BM$ blend films cast from chlorobenzene (CB) or CB + DIO.[10] In the CB-only case, the resulting $PC_{71}BM$-rich domains were quite large (≈200 nm) and exhibited a reasonably narrow size distribution, whereas with the addition of DIO, little if any phase separation was detected *via* BF-TEM imaging. In the case of DCB-processed films, BF-TEM yields no useful information.

Here we use energy-filtered TEM, which allows us to reliably image the phase separation present in processed films; using an approach based on hyperspectral imaging in conjunction with principal component analysis (PCA) that was described previously,[50] contrast was generated from the low-loss region of the electron energy loss spectrum. Plan-view images resulting from the PCA analysis are contained in the Supporting Information. EF-TEM tomography was then performed by collecting a tilt series of images acquired from the energy loss channels identified by PCA as those that generated maximum contrast from the two constituent phases. The results of EF-TEM tomographic reconstructions for DCB- and DCB/DIO-cast films are shown in Figure 5. In both cases, the $PC_{71}BM$-rich phase appears to form aggregates, with a PTB7-rich phase filling the spaces between. Notably, there are no obvious PTB7 crystal shapes such as nanofibrils, which are common for low molecular weight P3HT.

The EF-TEM tomography reveals a significant dependence of nanoscale morphology on the use of the DIO additive in DCB solution. Casting of blend films with DIO results in a more finely dispersed mixture of the PTB7-rich and $PC_{71}BM$-rich phases (Figure 5a). Specifically, the $PC_{71}BM$-rich domains in the film cast from DCB were found to exhibit a fairly heterogeneous size distribution, ranging in diameter from ≈20 to ≈100 nm. In contrast, the larger domains appear to be suppressed in the DIO-processed blend, resulting in a more homogeneous phase separation distance of ≈20 to ≈40 nm. This result may be surprising considering that the X-ray diffraction and spectroscopy experiments provide very little, if any, evidence of differences in the polymer order and orientation between these films. The difference in nanoscale morphology, therefore, may suggest an effect of the additive on the solidification/segregation behavior of the $PC_{71}BM$, rather than a significant impact on polymer solidification. The reduction in phase separation length scale, by itself, is likely the cause of much of the observed improvement in power conversion efficiency of devices processed with DIO.

SUMMARY

Polarizing spectroscopy and GIXD experiments, taken together, support the construction of a model which implies only very low content (≈20%) of crystalline donor polymer domains in the active layer of PTB7:$PC_{71}BM$ blend solar cells. Those crystalline polymer domains were found to have their (010) lattice planes oriented primarily out-of-plane, although the distribution of (010) orientations is broad, with the average (010) tilt at ≈33° from the film normal, and the correlation lengths for the crystals in the (010) direction are short (only on the order of a few to several π-stacked molecules). The polarizing spectroscopy experiments, which probe the polymer orientation in both crystalline and amorphous polymer, showed little overall preferential orientation, supporting the existence

of a majority fraction of amorphous polymer. While the X-ray scattering and polarizing spectroscopy experiments showed little difference between blend films prepared with and without DIO processing additive, a significant effect was observed using energy-filtered TEM. Specifically, the addition of DIO to the casting solvent (DCB) causes a decrease in the size-scale of the resulting interpenetrating BHJ structure.

These results suggest that caution should be taken before assuming that certain morphological features are necessary or sufficient conditions for good device performance. In the present case, it is not clear that nominal vertical orientation of π-stacking in PTB7 crystal domains is a sufficient reason to expect extraordinarily efficient extraction of photogenerated charges from a BHJ device, given the relatively low overall fraction of polymer that is crystalline. For the same reason, a high propensity to crystallize does not seem to be a necessary condition for an absorber polymer to enable high-performance OPV devices.

METHODS

Materials. PTB7 was synthesized as previously described.[9] $PC_{71}BM$, obtained from Nano-C Inc.,[44] was used as received.

Methods. PTB neat films were spuncast from 10 mg/mL solutions in *ortho*-dichlorobenzene (DCB), and BHJ films were spun-cast from DCB solutions with 13 mg/mL polymer loading. PTB7:$PC_{71}BM$ solutions had 1:1.2 polymer:fullerene mass ratio. Solutions were heated at 80 °C overnight and spun-cast (hot) at 83.8 radians/s (800 rpm) for 60 s. For blend films cast from DCB with diiodooctane (DIO) processing additive, the DIO constituted 3% (by volume) of the solvent. Samples were very nearly dry after spin-coating but were nonetheless allowed to dry for at least 10 min in the N_2 glovebox environment before packaging for transportation to subsequent experiments. Films were cast onto different substrates according to the needs of the subsequent analyses. Nearly always, the substrate surface was silicon oxide and was most typically native-oxide-covered silicon wafers. The one exception is that samples for EF-TEM analysis were spin-coated onto silicon wafers first coated with PEDOT:PSS (Clevios P VP Al 4083, H.C. Starck Inc.). After the PEDOT:PSS layer was annealed, the PTB7:$PC_{71}BM$ blend layer was spin-coated. After drying, the blend film was scored, floated onto the surface of deionized water, and picked up on a TEM grid.

Grazing-incidence X-ray diffraction was performed at beamline 11-3 at the Stanford Synchrotron Radiation Lightsource (SSRL), using a 12.7 keV primary beam, incident angles of 0.10 to 0.12° (between the critical angle of the film and the substrate), and a MAR345 image plate detector. The sample was enclosed in a helium-filled chamber to minimize air scattering and beam damage. Sample-to-detector distance (nominally 400 mm) was calibrated using the scattering pattern obtained from a LaB_6 calibration sample.

Ellipsometry experiments were performed using an M-2000 series spectroscopic ellipsometer (J.A. Woollam Co., Inc.). Measurements were made on films cast identically on three substrates. Films on silicon (native oxide) and silicon + silicon oxide (≈200 nm) substrates were measured at 45, 60, and 75° with respect to the film surface normal. Films on fused quartz substrates were measured twice: with the film side down (incident and reflected beams transmitted through the substrate, at 55, 60, 65, and 70°) and with the film facing up (45, 52.5, 60, 67.5, and 75°). Data sets were fit simultaneously using WVASE32 software. Dichroic ratio values ($\varepsilon''_{zz}/\varepsilon''_{x\text{-}y}$) were calculated for $672 < \lambda < 692$.

NEXAFS spectroscopy was performed at the NIST soft X-ray materials characterization facility (Beamline U7A) at Brookhaven National Laboratories' National Synchrotron Light Source (NSLS). Details of the analysis procedures for orientation characterization and for interfacial composition determination have been published elsewhere.[29,42]

Polarized FTIR spectroscopy was performed, as described previously,[29] on films cast on undoped, double-side polished silicon wafers. With the sample positioned at Brewster's angle with respect to the incident beam, transmission IR spectra were recorded, with the polarization of the incident beam controlled by a wire grid polarizer placed before the sample. Forward simulation of the dichroic ratio A_p/A_s, as a function of transition dipole tilt, for the various films was also performed as described previously,[29] and more information is contained in the Supporting Information.

Energy-filtered TEM (EF-TEM) was carried out using an FEI Titan 80-300 TEM/STEM operating at 300 kV, which was equipped with a Gatan 865 Tridiem imaging energy filter. EF-TEM hyperspectral images were acquired from 0 to 60 eV loss using a 10 eV energy-selecting slide, an energy step width of 2 eV, and an exposure time of 2 s per channel. PCA processing was carried out using AXSIA.[51] Electron tomography was performed using XPlor3D (FEI Co.) using a Saxton tilt scheme from −65° to +65° specimen tilt with a 1.5° tilt step at zero tilt. Images at each tilt were acquired at 19 and 29 eV loss, using a 5 eV slit and an exposure time of 5 s. The ratio of each of these images was then taken and used as the input for tomographic reconstruction *via* weighted backprojection in IMOD.[52]

Acknowledgment. M.R.H. thanks the National Research Council's Research Associateship Programs at NIST for financial support. L.P.Y. acknowledges Financial supports from NSF, University of Chicago, NSF-MRSEC, AFOSR, and DOE. Portions of this research were carried out at the Stanford Synchrotron Radiation Lightsource, a national user facility operated by Stanford University on behalf of the U.S. Department of Energy, Office of Basic Energy Sciences.

Supporting Information Available: Notes on the GIXD, p-IR, and NEXAFS analyses, quantum chemical calculations, calculations regarding the morphology model, further EF-TEM results, and details. This material is available free of charge *via* the Internet at http://pubs.acs.org.

REFERENCES AND NOTES

1. Brabec, C. J.; Hauch, J. A.; Schilinsky, P.; Waldauf, C. Production Aspects of Organic Photovoltaics and Their Impact on Commercialization of Devices. *MRS Bull.* **2005**, *30*, 50–52.
2. Janssen, R. A. J.; Hummelen, J. C.; Sariciftci, N. S. Polymer−Fullerene Bulk Heterojunction Solar Cells. *MRS Bull.* **2005**, *30*, 33–36.
3. Winder, C.; Matt, G.; Hummelen, J. C.; Janssen, R. A. J.; Sariciftci, N. S.; Brabec, C. J. Sensitization of Low Bandgap Polymer Bulk Heterojunction Solar Cells. *Thin Solid Films* **2002**, *403−404*, 373–379.
4. Svensson, M.; Zhang, F.; Veenstra, S. C.; Verhees, W. J. H.; Hummelen, J. C.; Kroon, J. M.; Inganäs, O.; Andersson, M. R. High-Performance Polymer Solar Cells of an Alternating Polyfluorene Copolymer and a Fullerene Derivative. *Adv. Mater.* **2003**, *15*, 988–991.
5. Mühlbacher, D.; Scharber, M.; Morana, M.; Zhu, Z.; Waller, D.; Gaudiana, R.; Brabec, C. High Photovoltaic Performance of a Low-Bandgap Polymer. *Adv. Mater.* **2006**, *18*, 2884–2889.
6. Wienk, M. M.; Turbiez, M.; Gilot, J.; Janssen, R. A. J. Narrow-Bandgap Diketo-Pyrrolo-Pyrrole Polymer Solar Cells: The Effect of Processing on the Performance. *Adv. Mater.* **2008**, *20*, 2556–2560.

7. Liang, Y.; Wu, Y.; Feng, D.; Tsai, S.-T.; Son, H.-J.; Li, G.; Yu, L. Development of New Semiconducting Polymers for High Performance Solar Cells. *J. Am. Chem. Soc.* **2009**, *131*, 56–57.
8. Dennler, G.; Scharber, M. C.; Brabec, C. J. Polymer-Fullerene Bulk-Heterojunction Solar Cells. *Adv. Mater.* **2009**, *21*, 1323–1338.
9. Liang, Y.; Feng, D.; Wu, Y.; Tsai, S.-T.; Li, G.; Ray, C.; Yu, L. Highly Efficient Solar Cell Polymers Developed *via* Fine-Tuning of Structural and Electronic Properties. *J. Am. Chem. Soc.* **2009**, *131*, 7792–7799.
10. Liang, Y.; Xu, Z.; Xia, J.; Tsai, S.-T.; Wu, Y.; Li, G.; Ray, C.; Yu, L. For the Bright Future—Bulk Heterojunction Polymer Solar Cells with Power Conversion Efficiency of 7.4%. *Adv. Mater.* **2010**, *22*, E135–E138.
11. Yang, X.; Loos, J. Toward High-Performance Polymer Solar Cells: The Importance of Morphology Control. *Macromolecules* **2007**, *40*, 1353–1362.
12. Sonar, P.; Singh, S. P.; Li, Y.; Soh, M. S.; Dodabalapur, A. A Low-Bandgap Diketopyrrolopyrrole-Benzothiadiazole-Based Copolymer for High-Mobility Ambipolar Organic Thin-Film Transistors. *Adv. Mater.* **2010**, *22*, 5409–5413.
13. Scharber, M. C.; Koppe, M.; Gao, J.; Cordella, F.; Loi, M. A.; Denk, P.; Morana, M.; Egelhaaf, H. J.; Forberich, K.; Dennler, G.; *et al.* Influence of the Bridging Atom on the Performance of a Low-Bandgap Bulk Heterojunction Solar Cell. *Adv. Mater.* **2009**, *22*, 367–370.
14. Li, G.; Shrotriya, V.; Huang, J.; Yao, Y.; Moriarty, T.; Emery, K.; Yang, Y. High-Efficiency Solution Processable Polymer Photovoltaic Cells by Self-Organization of Polymer Blends. *Nat. Mater.* **2005**, *4*, 864–868.
15. Erb, T.; Zhokhavets, U.; Gobsch, G.; Raleva, S.; Stühn, B.; Schilinsky, P.; Waldauf, C.; Brabec, C. J. Correlation between Structural and Optical Properties of Composite Polymer/Fullerene Films for Organic Solar Cells. *Adv. Funct. Mater.* **2005**, *15*, 1193–1196.
16. Li, G.; Shrotriya, V.; Yao, Y.; Huang, J.; Yang, Y. Manipulating Regioregular Poly(3-hexylthiophene):[6,6]-Phenyl-C61-butyric Acid Methyl Ester Blends—Route towards High Efficiency Polymer Solar Cells. *J. Mater. Chem.* **2007**, *17*, 3126–3140.
17. Salleo, A.; Kline, R. J.; DeLongchamp, D. M.; Chabinyc, M. L. Microstructural Characterization and Charge Transport in Thin Films of Conjugated Polymers. *Adv. Mater.* **2010**, *22*, 3812–3838.
18. McCulloch, I.; Heeney, M.; Bailey, C.; Genevicius, K.; MacDonald, I.; Shkunov, M.; Sparrowe, D.; Tierney, S.; Wagner, R.; Zhang, W.; *et al.* Liquid-Crystalline Semiconducting Polymers with High Charge-Carrier Mobility. *Nat. Mater.* **2006**, *5*, 328–333.
19. Chabinyc, M. L.; Toney, M. F.; Kline, R. J.; McCulloch, I.; Heeney, M. X-ray Scattering Study of Thin Films of Poly(2,5-bis(3-alkylthiophen-2-yl)thieno[3,2-*b*]thiophene. *J. Am. Chem. Soc.* **2007**, *129*, 3226–3237.
20. DeLongchamp, D.; Kline, R.; Lin, E.; Fischer, D.; Richter, L.; Lucas, L.; Heeney, M.; McCulloch, I.; Northrup, J. High Carrier Mobility Polythiophene Thin Films: Structure Determination by Experiment and Theory. *Adv. Mater.* **2007**, *19*, 833–837.
21. Rivnay, J.; Noriega, R.; Northrup, J. E.; Kline, R. J.; Toney, M. F.; Salleo, A. Structural Origin of Gap States in Semicrystalline Polymers and the Implications for Charge Transport. *Phys. Rev. B* **2011**, *83*, 121306.
22. Although the ordered regions of PTB7 are almost certainly highly paracrystalline, for the sake of readability in this report, we will often simply use the terms "crystal", "crystalline", or "crystallinity" and note here the caveat that we are taking a very broad definition of those terms. Technically, it would be more precise, albeit cumbersome, to discuss "regions of polymer ordered enough to give rise to measurable X-ray diffraction peaks (as opposed to broad amorphous scattering)".
23. Gomez, E. D.; Barteau, K. P.; Wang, H.; Toney, M. F.; Loo, Y.-L. Correlating the Scattered Intensities of P3HT and PCBM to the Current Densities of Polymer Solar Cells. *Chem. Commun.* **2010**, *47*, 436–438.
24. Rivnay, J.; Steyrleuthner, R.; Jimison, L. H.; Casadei, A.; Chen, Z.; Toney, M. F.; Facchetti, A.; Neher, D.; Salleo, A. Drastic Control of Texture in a High Performance n-Type Polymeric Semiconductor and Implications for Charge Transport. *Macromolecules* **2011**, *44*, 5246–5255.
25. Jimison, L. H. Understanding Microstructure and Charge Transport in Semicrystalline Polythiophenes. Ph.D. Thesis, Stanford University, Palo Alto, California, 2011.
26. Guo, J.; Liang, Y.; Szarko, J.; Lee, B.; Son, H. J.; Rolczynski, B. S.; Yu, L.; Chen, L. X. Structure, Dynamics, and Power Conversion Efficiency Correlations in a New Low Bandgap Polymer: PCBM Solar Cell. *J. Phys. Chem. B* **2009**, *114*, 742–748.
27. Verploegen, E.; Mondal, R.; Bettinger, C. J.; Sok, S.; Toney, M. F.; Bao, Z. Effects of Thermal Annealing upon the Morphology of Polymer–Fullerene Blends. *Adv. Funct. Mater.* **2010**, *20*, 3519–3529.
28. Baker, J. L.; Jimison, L. H.; Mannsfeld, S.; Volkman, S.; Yin, S.; Subramanian, V.; Salleo, A.; Alivisatos, A. P.; Toney, M. F. Quantification of Thin Film Crystallographic Orientation Using X-ray Diffraction with an Area Detector. *Langmuir* **2010**, *26*, 9146–9151.
29. Gurau, M. C.; Delongchamp, D. M.; Vogel, B. M.; Lin, E. K.; Fischer, D. A.; Sambasivan, S.; Richter, L. J. Measuring Molecular Order in Poly(3-alkylthiophene) Thin Films with Polarizing Spectroscopies. *Langmuir* **2007**, *23*, 834–842.
30. Park, S. H.; Roy, A.; Beaupre, S.; Cho, S.; Coates, N.; Moon, J. S.; Moses, D.; Leclerc, M.; Lee, K.; Heeger, A. J. Bulk Heterojunction Solar Cells with Internal Quantum Efficiency Approaching 100%. *Nat. Photonics* **2009**, *3*, 297–302.
31. Cho, S.; Seo, J. H.; Park, S. H.; Beaupré, S.; Leclerc, M.; Heeger, A. J. A Thermally Stable Semiconducting Polymer. *Adv. Mater.* **2010**, *22*, 1253–1257.
32. See especially data in the Supporting Information for the preceding reference.
33. Beiley, Z. M.; Hoke, E. T.; Noriega, R.; Dacuna, J.; Burkhard, G. F.; Bartelt, J. A.; Salleo, A.; Toney, M. F.; McGehee, M. D. Morphology-Dependent Trap Formation in High Performance Polymer Bulk Heterojunction Solar Cells. *Adv. Funct. Mater.* **2011**, *1*, 954–962.
34. Peet, J.; Cho, N. S.; Lee, S. K.; Bazan, G. C. Transition from Solution to the Solid State in Polymer Solar Cells Cast from Mixed Solvents. *Macromolecules* **2008**, *41*, 8655–8659.
35. Di Nuzzo, D.; Aguirre, A.; Shahid, M.; Gevaerts, V. S.; Meskers, S. C. J.; Janssen, R. A. J. Improved Film Morphology Reduces Charge Carrier Recombination into the Triplet Excited State in a Small Bandgap Polymer–Fullerene Photovoltaic Cell. *Adv. Mater.* **2010**, *22*, 4321–4324.
36. The batch of PTB7 used here had a number-average molecular weight of 42 kg/mol and a PDI of 2.2. Devices made with this batch showed power conversion efficiencies above 7%.
37. Szarko, J. M.; Guo, J.; Liang, Y.; Lee, B.; Rolczynski, B. S.; Strzalka, J.; Xu, T.; Loser, S.; Marks, T. J.; Yu, L.; *et al.* When Function Follows Form: Effects of Donor Copolymer Side Chains on Film Morphology and BHJ Solar Cell Performance. *Adv. Mater.* **2011**, *22*, 5468–5472.
38. A pole figure is a graphical representation of the distribution of orientations of a set of crystallographic planes.
39. Smilgies, D.-M. Scherrer Grain-Size Analysis Adapted to Grazing-Incidence Scattering with Area Detectors. *J. Appl. Crystallogr.* **2009**, *42*, 1030–1034.
40. Lilliu, S.; Agostinelli, T.; Pires, E.; Hampton, M.; Nelson, J.; Macdonald, J. E. Dynamics of Crystallization and Disorder during Annealing of P3HT/PCBM Bulk Heterojunctions. *Macromolecules* **2011**, *44*, 2725–2734.
41. The quoted uncertainty in the relative crystallinity represents the standard deviation and is based on uncertainty in the fits of the (overlapping) diffraction peaks, as well as uncertainty in film thicknesses.
42. Germack, D. S.; Chan, C. K.; Kline, R. J.; Fischer, D. A.; Gundlach, D. J.; Toney, M. F.; Richter, L. J.; DeLongchamp, D. M. Interfacial Segregation in Polymer/Fullerene Blend Films for Photovoltaic Devices. *Macromolecules* **2010**, *43*, 3828–3836.

43. Tammer, M.; Monkman, A. P. Measurement of the Anisotropic Refractive Indices of Spin Cast Thin Poly(2-methoxy-5-(2′-ethylhexyloxy)-*p*-phenylenevinylene) (MEH−PPV) Films. *Adv. Mater.* **2002**, *14*, 210–212.
44. Certain commercial equipment, instruments, computer programs, or materials are identified in this paper to foster understanding. Such identification does not imply recommendation or endorsement by the National Institute of Standards and Technology nor does it imply that the materials or equipment identified are necessarily the best available for this purpose.
45. Snyder, R. G.; Strauss, H. L.; Elliger, C. A. Carbon−Hydrogen Stretching Modes and the Structure of *n*-Alkyl Chains. 1. Long, Disordered Chains. *J. Phys. Chem.* **1982**, *86*, 5145–5150.
46. Germack, D. S.; Chan, C. K.; Hamadani, B. H.; Richter, L. J.; Fischer, D. A.; Gundlach, D. J.; DeLongchamp, D. M. Substrate-Dependent Interface Composition and Charge Transport in Films for Organic Photovoltaics. *Appl. Phys. Lett.* **2009**, *94*, 233303-3.
47. DeLongchamp, D. M.; Kline, R. J.; Fischer, D. A.; Richter, L. J.; Toney, M. F. Molecular Characterization of Organic Electronic Films. *Adv. Mater.* **2011**, *23*, 319–337.
48. Levy, O.; Stroud, D. A Maxwell−Garnett Theory for Mixtures of Anisotropic Inclusions: Applications to Conducting Polymers. *Phys. Rev. B* **1997**, *56*, 8035–8046.
49. Clark, J.; Chang, J.-F.; Spano, F. C.; Friend, R. H.; Silva, C. Determining Exciton Bandwidth and Film Microstructure in Polythiophene Films Using Linear Absorption Spectroscopy. *Appl. Phys. Lett.* **2009**, *94*, 163306.
50. Herzing, A. A.; Richter, L. J.; Anderson, I. M. 3D Nanoscale Characterization of Thin-Film Organic Photovoltaic Device Structures *via* Spectroscopic Contrast in the TEM. *J. Phys. Chem. C* **2010**, *114*, 17501–17508.
51. Kotula, P. G.; Keenan, M. R.; Michael, J. R. Automated Analysis of SEM X-ray Spectral Images: A Powerful New Microanalysis Tool. *Microsc. Microanal.* **2003**, *9*, 1–17.
52. Kremer, J. R.; Mastronarde, D. N.; McIntosh, J. R. Computer Visualization of Three-Dimensional Image Data Using IMOD. *J. Struct. Biol.* **1996**, *116*, 71–76.